

Moving Integration Filter-Based Open-Switch Fault Diagnosis Method for Three-phase Induction Motor Drive Systems

Shuqi Shi, Yao Sun, *Member, IEEE*, Xing Li, Hanbing Dan, Mei, Su, *Member, IEEE*

Abstract—Reliable fault diagnosis is essential to the induction motor drive systems in some special applications. In this paper, we present a simple and robust fault diagnosis scheme for three-phase induction motor drive systems. As the proposed fault diagnosis method is based on the framework of model predictive control, many shared data can be fully utilized, the computation burden is greatly reduced. To improve the robustness of fault detection, a moving integration filter-based residuals construction method is proposed, which reduces both the false alarms rate and the rate of missed detection. According to the order of the constructed residuals and the sign of current errors, it is easy to accomplish the task of fault isolation. Experimental results are presented to demonstrate the effectiveness of the proposed fault diagnosis method.

Index Terms—Fault diagnosis, induction motor drive, model predictive control, moving integration filter.

I. INTRODUCTION

THE AC induction motors have been widely used in industry, agriculture, transportation and household users. In most modern AC induction motors drive systems, related power converters have become important parts and played a crucial role in the reliability of the entire drive system [1]-[4].

It has been reported that more than 30% of the electrical faults in the AC drive systems are power circuit faults [3]. And most of them are semiconductor device faults, such as open-switch and short-circuit faults. The diagnosis of short circuit

fault is mostly based on the design of hardware circuit, which has been summarized in [5]. The fast fuse can also be implanted in the inverter circuit, and the short-circuit fault of the power tube can be transformed into an open circuit. Then the open circuit diagnosis method can be used to deal with it.

Usually, AC drive systems are sensitive to semiconductor device faults. Once the semiconductor device failures occur, they must be handled in time. Otherwise, it may result in great economic loss and safety accidents, especially in some applications with high-security requirements. Therefore, it is important to accurately detect and isolate the faults, which also lays a solid foundation for the implementation of fault-tolerant measures [6]-[8].

In recent years, the open-switch faults have received much attention and lots of methods have been presented to detect and isolate these faults in the power converters. According to their characteristics, they could be mainly classified into two categories by the measured variables: current-based [9]-[17] and voltage-based methods [18]-[24].

The current-based methods have been widely proposed, which can be mainly classified into the average current methods, the slope methods and the current observer-based methods. The average current methods [9]-[10] detect the open-switch faults from the mean value of output currents over one fundamental period. In [9], it uses the average motor currents Park's vector in the stator frame to monitor switch faults, applying Clarke's transformation. However, it has a disadvantage of load dependence. To overcome this problem, the normalized average currents were suggested and refined in [11] and [12]. In [11], the robustness of the fault diagnosis method was enhanced, and the detection of multiple faults was achieved. A fault diagnosis method based on the calculation of the errors of the normalized currents' average absolute values was proposed in [12], where the independence of the mechanical operating conditions and immunity to false alarms were demonstrated by choosing the Park's vector modulus as normalization quantity. As to the slope methods [13]-[14], the faults can be identified by the slope of the current vector trajectory, which is assumed to be constant for a quarter of current period. And to further locate the fault switches, the Schmitt Triggers are utilized to detect the polarity of the currents during the faults. Compared with the previous methods, the current observer-based method [15]-[17]

Manuscript received January 8, 2020; revised April 7, 2020; accepted May 23, 2020. This work was supported in part by the National Natural Science Foundation of China under Grant 61622311, 61933011 and 61903382, in part by the Project of Innovation-driven Plan in Central South University under Grant 2019CX003, in part by the Major Project of Changzhutan Self-dependent Innovation Demonstration Area under Grant 2018XK2002. (*Corresponding author: Hanbing Dan.*)

Shuqi Shi is with the School of Automation, Central South University, Changsha 410083, China, and also with the Hunan Provincial Key Laboratory of Grids Operation and Control on Multi-Power Sources Area, Shaoyang University, Shaoyang, 422000, China (e-mail: 382963054@qq.com).

Yao Sun, Hanbing Dan and Mei Su are with the School of Automation, Central South University, Changsha 410083, China (e-mail: yaosuncsu@gmail.com; daniel698@sina.com; sumeicsu@csu.edu.cn).

Xing Li is with the College of Electrical and Information Engineering Hunan University, Changsha 410082, China (e-mail: lxhnu@hnu.edu.cn).

can effectively reduce the time of fault detection. In [15], a current residual vector-based approach is proposed. This method uses the current residual between the measured and estimated value to detect the fault. It eliminates the impact of the load variations and control strategy, reducing the detection time to one-quarter of the fundamental period. [16]-[17] proposed a fast detection method based on the observed value of the current deviation and an extra voltage test procedure. It only needs a few switching cycles to detect the open-switch faults, even in the case of transient operation.

In general, the principle of voltage-based methods is that the fault is diagnosed by examining the deviation between normal and abnormal conditions. Many early voltage-based methods usually require additional voltage sensors, compared with the current-based approaches.

Four fault detection techniques based on voltage method are proposed in [18]. By analyzing the model of the converter, these detection methods are achieved by comparing the key points' voltages measurements with their corresponding references. But it requires multiple voltage sensors and the detection time is a fourth of the fundamental cycle. In [19], a fast fault diagnosis method based on the line-to-line voltage measurement is proposed, which can detect the single and multiple open-switch faults by two voltage sensors. To avoid the additional voltage sensors, [20] proposes a fault diagnosis algorithm for the micro-grids inverters based on the waveform characteristics and composition analysis of the main fault component. But its detection time is long. In order to reduce the detection time, some fault detection methods [21]-[23] based on finite set model predictive control are proposed, which can detect the open-switch fault with several switching cycles. In [21], an error-voltage-based open-switch fault-diagnosis strategy with a finite set model predictive control method has been investigated. [22] proposes a fast fault detection and isolation approach to identify single open-circuit faults with model-predictive control. The fault detection approach is simply implemented by checking the voltage errors between the measured arm voltages and the estimated ones in the former control cycle. Besides, the intelligent technology method [24] is also introduced to detect the faults in the multilevel inverters. It can ignore the influence of the system non-linear factors. However, it requires complicated calculations that are not easy to implement in actual controllers.

In this paper, a simple and reliable open-switch fault diagnosis technique based on moving integration filters is proposed. And its advantages are summarized as follows:

- 1) No extra sensors are required, which does not increase additional cost;
- 2) The computation cost of this fault diagnosis method is small. Since the fault diagnosis method is based on the framework of model predictive control, many shared data could be fully utilized, the computation burden of this fault diagnosis method is small;
- 3) This method is robust and reliable. As the moving integration filter-based residuals are used, it is easy to find a threshold to ensure a low rate of false alarm and missed detection.

The remainder of this paper is organized as follows: Section II presents the mathematical model of the studied three-phase induction drive system. The proposed finite-set model predictive control scheme of the induction motor drive system is demonstrated in Section III. Section IV elaborates the proposed fault diagnosis strategy in detail. The experimental results are shown in Section V. Finally, the conclusion is presented in Section VI.

II. THREE-PHASE INDUCTION MOTOR DRIVE SYSTEM

The circuit topology of the three-phase induction drive system is illustrated in Fig. 1, which is made up of a single-phase to three-phase inverter and an induction machine. In this system, the single-phase rectifier provides a dc-link voltage and realizes power factor correction, and the three-phase inverter feeds a three-phase induction motor.

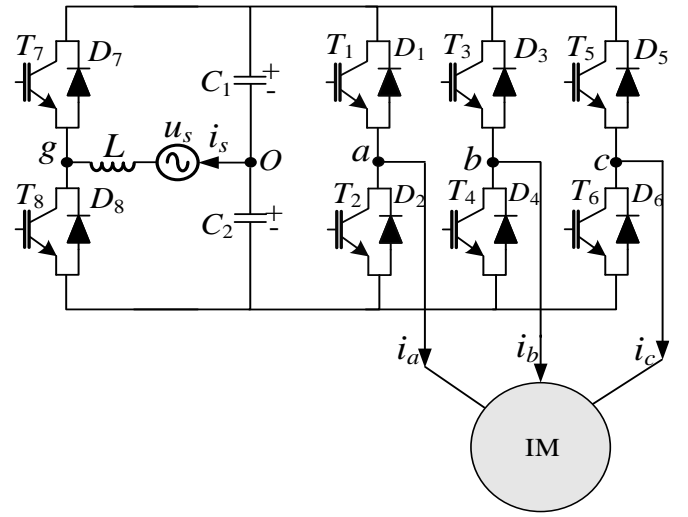


Fig. 1. Three-phase induction motor drive system.

For convenience, we define S_i ($i=1, 2, 3, 4, 5, 6, 7, 8$) as the switching state of the switch T_i in the converter. Then the dynamic equations of the drive system are expressed as follows

$$\begin{cases} C \frac{du_{c1}}{dt} = S_7 i_s - S_1 i_a - S_3 i_b - S_5 i_c \\ C \frac{du_{c2}}{dt} = S_2 i_a + S_4 i_b + S_6 i_c - S_8 i_s \\ L \frac{di_s}{dt} = u_s - S_7 u_{c1} + S_8 u_{c2} \end{cases} \quad (1)$$

where L is the inductance on the grid side, i_s and u_s are ac line current and grid voltage, respectively. $C_1 = C_2 = C$ is the capacitor of DC-link, u_{c1} and u_{c2} are the voltage across capacitance C_1 and C_2 , respectively.

$$\begin{cases} L_{\delta} \frac{di_a}{dt} = S_1 u_{c1} - S_2 u_{c2} - R i_a - e_a - u_{no} \\ L_{\delta} \frac{di_b}{dt} = S_3 u_{c1} - S_4 u_{c2} - R i_b - e_b - u_{no} \\ L_{\delta} \frac{di_c}{dt} = S_5 u_{c1} - S_6 u_{c2} - R i_c - e_c - u_{no} \\ \frac{L_m}{L_r} \frac{d\psi_{ri}}{dt} = e_i, i \in (a, b, c) \end{cases} \quad (2)$$

$$u_{no} = \frac{(S_1 + S_3 + S_5)u_{c1} - (S_2 + S_4 + S_6)u_{c2}}{3} \quad (3)$$

where i_i , e_i and ψ_{ri} ($i=a, b, c$) represent the stator currents, back electromotive force and rotor flux of the induction machine, respectively. L_{δ} , L_m , L_r and R refer to the leakage inductance, mutual inductance, rotor inductance and stator resistance of the machine, respectively.

III. MODEL PREDICTIVE CONTROL OF INDUCTION MOTOR DRIVE SYSTEM

Finite-set model predictive control is widely used in systems related to power electronics due to its advantages of easy to implement and handle constraints [25]-[26]. In this study, it is applied to the current control of the induction motor drive system. To reduce the computation burden and eliminate the weighting coefficients, the control system is divided into two parts: model predictive control of single-phase rectifier and model predictive control of induction motor.

A. Discrete Model of Current Dynamics

To implement the model predictive control, the current dynamics should be discretized. For simplicity, forward Euler discretization is used in this study.

The discrete model of input current (Model A) is expressed as

$$i_s^p = i_s(k) + \frac{T_s}{L} [u_s(k) - S_7(k)u_{c1}(k) + S_8(k)u_{c2}(k)] \quad (4)$$

From (2), the discrete model of the stator currents (Model B) is as follows

$$\begin{cases} i_a^p = i_a(k) + \frac{T_s}{L_{\delta}} [S_1(k)u_{c1}(k) - S_2(k)u_{c2}(k) \\ \quad - R i_a(k) - e_a(k) - u_{no}(k)] \\ i_b^p = i_b(k) + \frac{T_s}{L_{\delta}} [S_3(k)u_{c1}(k) - S_4(k)u_{c2}(k) \\ \quad - R i_b(k) - e_b(k) - u_{no}(k)] \\ i_c^p = i_c(k) + \frac{T_s}{L_{\delta}} [S_5(k)u_{c1}(k) - S_6(k)u_{c2}(k) \\ \quad - R i_c(k) - e_c(k) - u_{no}(k)] \end{cases} \quad (5)$$

where T_s is the sampling period. The variables with superscript p mean the predicted values.

B. Control Scheme of Single-Phase Rectifier

The control targets of the rectifier include power factor correction, dc-link voltage regulation and midpoint capacitor

voltage balance. Thus, the designed control block diagram includes a dc-link voltage controller, a voltage balancing controller and a current controller, which is shown in Fig.2.

As this is a single-phase rectifier, the inherent twice power ripple may degrade control performance. To mitigate the negative effect of the twice power ripple, a notch filter (notch₁) with the resonance frequency of 100Hz is applied to the dc-link voltage feedback signal. In addition, the voltage balancing on average between C_1 and C_2 must be guaranteed. Since the voltage difference between C_1 and C_2 contains an AC component with the fundamental frequency, a notch filter (notch₂) with the resonance frequency of 50Hz is used in the voltage balancing controller.

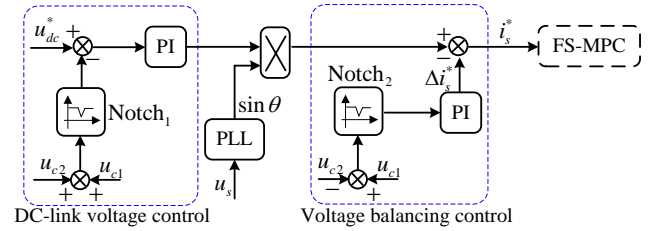


Fig. 2. Control schematic diagram of rectifier.

For the purpose of fast dynamic response, the idea of finite set model predictive control (FS-MPC) is applied in the current loop of the rectifier, and its total minimum cost function is designed as

$$\begin{cases} G_1 = \varepsilon_s^2 \\ \varepsilon_s = i_s^* - i_s^p \end{cases} \quad (6)$$

C. Control Scheme of Induction Motor

In this section the classic field-oriented control is applied to the induction motor [27]. The related control block diagram is shown in Fig. 3, where the rotor flux is obtained by a flux observer, the speed tracking is realized by a proportional-integral control, and the currents are controlled by a finite-set model predictive controller.

To track the current reference values well, we should minimize current errors between the references and the predicted values. And the errors $[\varepsilon_a, \varepsilon_b, \varepsilon_c]$ are expressed as

$$\begin{cases} \varepsilon_a = i_a^* - i_a^p \\ \varepsilon_b = i_b^* - i_b^p \\ \varepsilon_c = i_c^* - i_c^p \end{cases} \quad (7)$$

As the sum of the three-phase currents is zero, any two errors above should be minimized. Thus, the cost function for the model predictive control is expressed as

$$G_2 = \varepsilon_a^2 + \varepsilon_b^2 \quad (8)$$

The flow chart of the proposed model predictive control algorithm is shown in Fig. 4. Where $X = [S_7, S_8]$ denotes the switching state combination of rectifier, and "k" represents the kth switching state of the two options. X_{OP} represents the

optimal switching state chosen by module ‘Switch State Selection 1’, and it is used for the next control period. G_{10P} and G_{10} are the minimum and initial values of the cost function G_1 , respectively. Where $S = [S_1, S_2, S_3, S_4, S_5, S_6]$ denotes the switching state combination of inverter, and “ j ” represents the

j th switching state of the eight options. S_{OP} represents the optimal switching state chosen by module ‘Switch State Selection’, and it is used for the next control period. G_{20P} and G_{20} are the minimum and initial values of the cost function G_2 , respectively.

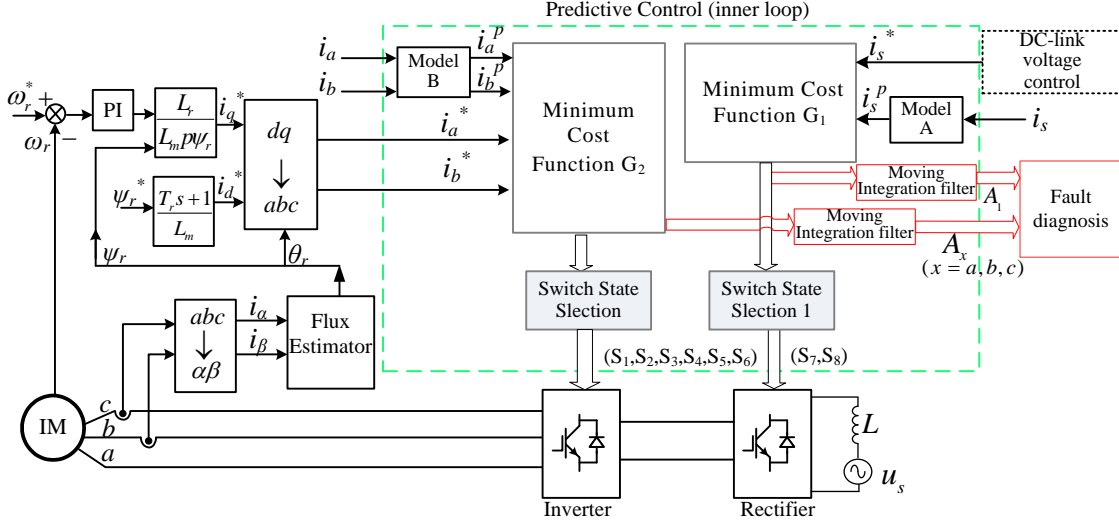


Fig. 3. Overall control block diagram of proposed scheme.

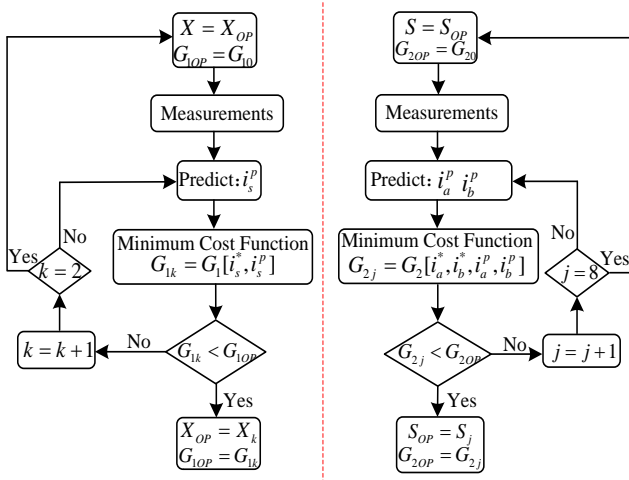


Fig. 4. Flow chart of finite-set model predictive control.

IV. PROPOSED FAULT DIAGNOSIS METHOD

A. Fault Diagnosis Method of Rectifier

When an open-circuit fault happens on a switch of the rectifier and the associated current direction meets some condition, then the rectifier may lose controllability. As a result, the value of the associated cost function under the model predictive control will be greater than that in normal condition, which is the basis of the proposed fault detection method. To

show two types of faults and their effect on system performance, Fig. 5 shows the situation when T_7 and T_8 occur open-switch fault respectively. For better understanding, assuming that an open-circuit fault occurs at T_7 at $t=t_a$, the related waveforms are shown in Fig. 5. As seen, when i_s^* is greater than zero, the related G_1 is not affected by the fault. When i_s^* is less than zero, the predicted current i_s^p is almost clamped to zero, and an obvious change can be found about G_1 . A similar phenomenon can also be found when an open-circuit fault occurs at T_8 . Intuitively, we could construct such a criterion for fault detection as follows.

$$Status = \begin{cases} F & G_1 > k_{m1} \\ N & otherwise \end{cases} \quad (9)$$

where k_{m1} is a threshold value, the status ‘F’ means fault state and ‘N’ means normal state. As well known, a good fault diagnosis criterion should guarantee that the false alarm rate under extreme cases is small and a true fault must be detected definitely. It is clear that a large k_{m1} will help to reduce the false alarm rate, but it may increase the rate of missed detection. For instance, when the system works under light load, the true fault may be missed.

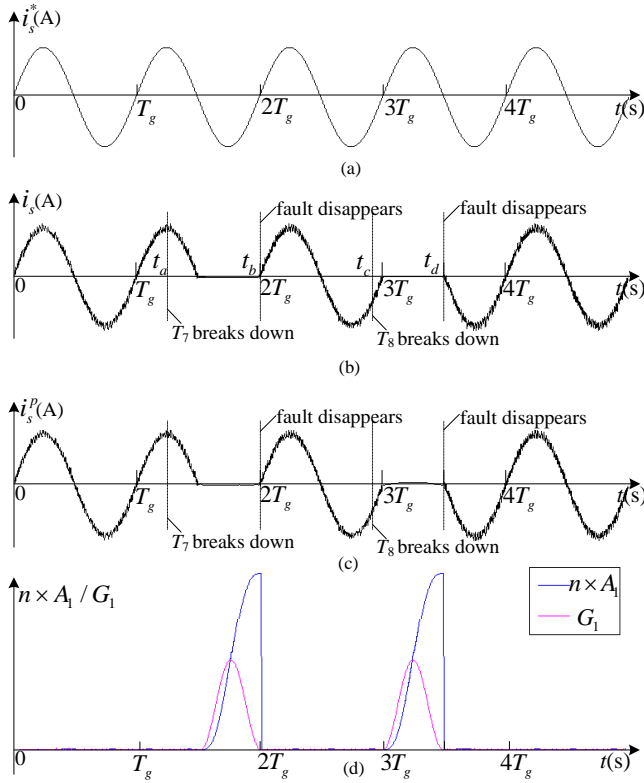


Fig. 5. Waveforms with an open-switch fault in rectifier. (a) input current reference; (b) input current; (c) predicted input current; (d) residuals.

To address the contradiction above, the criterion is modified as follows.

$$Status = \begin{cases} F & A_1 > k_{m1} \\ N & otherwise \end{cases} \quad (10)$$

where A_1 is the output of a moving integration filter. The moving integration filter is expressed as

$$A_1 = \int_{t-T_g/2}^t \varepsilon_s^2(\tau) d\tau \quad (11)$$

where T_g is the fundamental period of grid voltages.

The discrete-time equation of (11) is described as

$$A_1(k) = A_1(k-1) + T_s(\varepsilon_s^2(k) - \varepsilon_s^2(k-n)) \quad (12)$$

where n is equal to $T_g/(2T_s)$.

To distinguish double open-circuit faults more easily, A_1 is reset at each zero-crossing point of the current reference. From Fig. 5, it is clear that the change of A_1 during fault is larger than G_1 . Thus, it gives more choice to determine the threshold value.

Fault isolation is another task in fault diagnosis. To finish this task, the error ε_s will be used. From Fig.5, it can be observed that when the fault happens on T_7 , $\varepsilon_s < 0$, and while it happens on T_8 , $\varepsilon_s > 0$. Thus, the overall fault diagnosis algorithm is listed in Table I. The corresponding flow chart of the proposed single fault diagnosis of rectifier is shown in Fig.6.

TABLE I
FAULT SWITCH DIAGNOSTIC TABLE FOR RECTIFIER

Single Open-switch Faults	Fault switch	Double Open-switch Faults	Fault switch
$A_1 < k_{m1}$	—		
$\begin{cases} A_1 > k_{m1} \\ \varepsilon_s > 0 \end{cases} \Leftrightarrow \text{I}$	T_7	I && II	T_7, T_8
$\begin{cases} A_1 > k_{m2} \\ \varepsilon_s < 0 \end{cases} \Leftrightarrow \text{II}$	T_8		

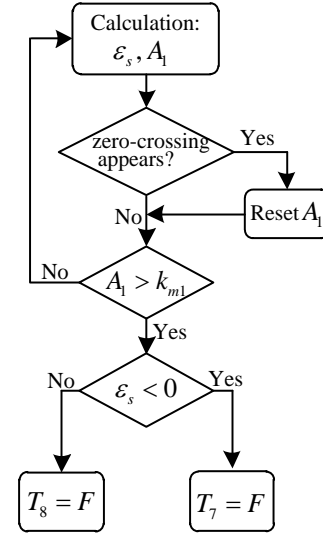


Fig. 6. Flow chart of proposed fault diagnosis for rectifier.

B. The Fault Diagnosis Method of Inverter

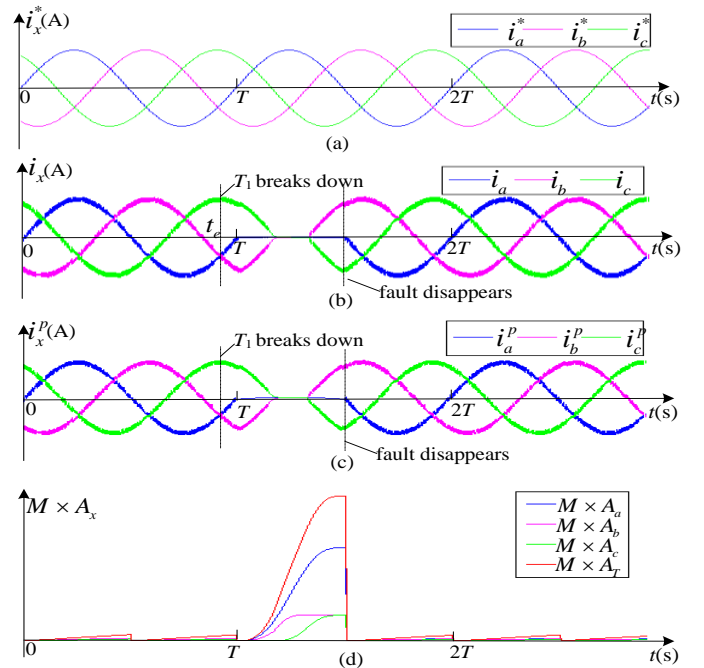


Fig. 7. Waveforms with an open-switch fault in inverter. (a) output current reference; (b) actual output current; (c) predicted output current; (d) residuals.

Take the phase- a as an example. According to (5), the error between the predicted current and the actual current is

$$\begin{aligned} & i_a^p - i_a(k) \\ & = \frac{T_s}{L_s} [S_1(k)u_{c1}(k) - S_2(k)u_{c2}(k) - Ri_a(k) - e_a(k) - u_{no}(k)] \end{aligned} \quad (13)$$

In normal conditions, since the system is controllable, the predicted current is approximately equal to the actual current. When the switch T_1 of phase- a is faulty, the predicted output voltage is different from its actual value. However, the error is small. The main reason is that T_s / L_s is relatively small. Simulation results are shown in Fig. 7, where the predicted currents are similar to the actual ones.

To realize the target of fault detection, the following variables are defined firstly:

$$A_x = \int_{t-T}^t \varepsilon_x^2(\tau) d\tau, \quad (x = a, b, c) \quad (14)$$

$$A_T = \sum_{a,b,c} A_x \quad (15)$$

where A_x is obtained by passing the square of the current error to a moving integration filter, A_T is the sum of A_x . T is the output current period of the inverter. In the induction motor drive system, the period could be obtained by a phase-locked loop (PLL) whose inputs are the estimated rotor flux [28]-[29].

The discrete-time equation of (14) is described as

$$A_x(k) = A_x(k-1) + T_s(\varepsilon_x^2(k) - \varepsilon_x^2(k-M)) \quad (16)$$

where M is equal to $T/(2T_s)$. To distinguish double open-circuit faults more easily, A_a , A_b and A_c are reset to zero at the zero-crossing point of phase- a reference current in normal operation. After a faulty phase is detected, they are reset to zero at the zero-crossing point of faulty phase reference current.

The proposed criterion of open-switch fault detection for the inverter is

$$Status = \begin{cases} F & A_T > k_m \\ N & otherwise \end{cases} \quad (17)$$

where k_m is a threshold value.

Different from the rectifier, the three-phase currents of the inverter are interdependent of each other and the number of switches is larger. Thus, it is more difficult to realize the fault isolation of the inverter. To determine the position of the fault switch, we divide the process into two steps. Firstly, we determine the phase number of the inverter where the fault switch occurs. Secondly, we determine the specific location of the fault switch (top switch or bottom switch).

In the first step, compare the residuals A_a , A_b and A_c and find the largest one. The phase with the largest value is the one with fault. In the second step, the specific location of the fault switch is determined by judging the sign of error ε_x . If $\varepsilon_x > 0$, the top switch is broken; otherwise, the bottom one is broken. Summarizing the fault detection and fault isolation method before, the corresponding fault switch diagnostic table shown in Table II is obtained. And the overall flow chart of the proposed single open-switch fault diagnosis of inverter is shown in Fig. 8.

Note that Fig. 6 and Fig. 8 only show the cases with single open-switch faults. With regard to the fault diagnosis of double

open-circuit faults, we need to repeat the procedure in Fig. 6 or Fig. 8 and combine the adjacent diagnostic results to give the final decision.

TABLE II
FAULT SWITCH DIAGNOSTIC TABLE FOR INVERTER

Single Open-switch Faults	Fault switch	Double Open-switch Faults	Fault switch
$\begin{cases} A_a < k_{m2} \\ A_b < k_{m2} \\ A_c < k_{m2} \end{cases}$	—	①&&②	T_1, T_2
		①&&③	T_1, T_3
		①&&④	T_1, T_4
$\begin{cases} A_T > k_{m2} \\ A_a > A_b \&\& A_a > A_c \\ \varepsilon_a > 0 \end{cases} \Leftrightarrow \textcircled{1}$	T_1	①&&⑤	T_1, T_5
		①&&⑥	T_1, T_6
$\begin{cases} A_T > k_{m2} \\ A_a > A_b \&\& A_a > A_c \\ \varepsilon_a < 0 \end{cases} \Leftrightarrow \textcircled{2}$	T_2	②&&③	T_2, T_3
		②&&④	T_2, T_4
$\begin{cases} A_T > k_{m2} \\ A_b > A_a \&\& A_b > A_c \\ \varepsilon_b > 0 \end{cases} \Leftrightarrow \textcircled{3}$	T_3	②&&⑤	T_2, T_5
		②&&⑥	T_2, T_6
$\begin{cases} A_T > k_{m2} \\ A_b > A_a \&\& A_b > A_c \\ \varepsilon_b < 0 \end{cases} \Leftrightarrow \textcircled{4}$	T_4	③&&④	T_3, T_4
		③&&⑤	T_3, T_5
$\begin{cases} A_T > k_{m2} \\ A_c > A_a \&\& A_c > A_b \\ \varepsilon_c > 0 \end{cases} \Leftrightarrow \textcircled{5}$	T_5	③&&⑥	T_3, T_6
		④&&⑤	T_4, T_5
$\begin{cases} A_T > k_{m2} \\ A_c > A_a \&\& A_c > A_b \\ \varepsilon_c < 0 \end{cases} \Leftrightarrow \textcircled{6}$	T_6	④&&⑥	T_4, T_6
		⑤&&⑥	T_5, T_6

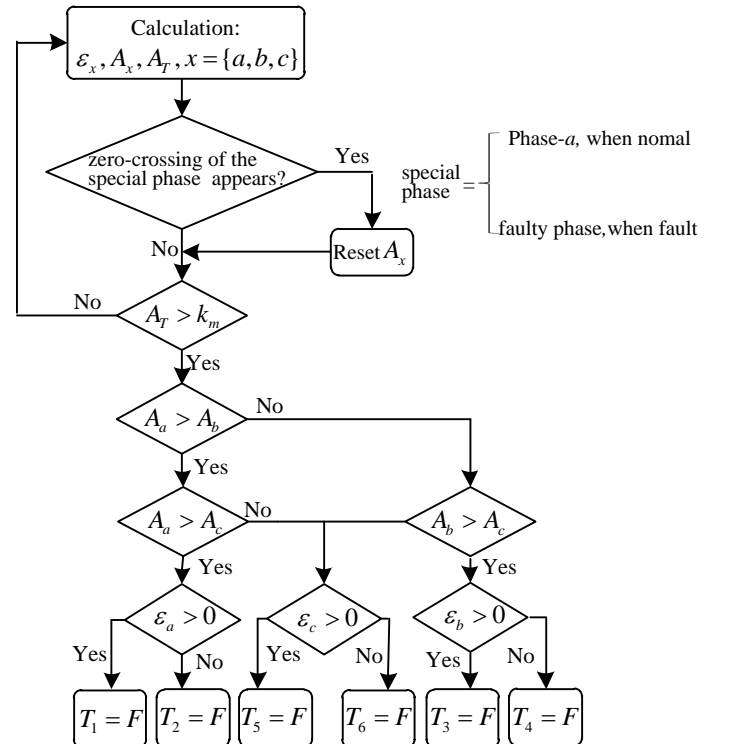


Fig. 8. Flow chart of proposed fault diagnosis for inverter.

V. EXPERIMENTAL RESULTS

In order to verify the effectiveness of the proposed fault

diagnosis strategy, an experimental prototype shown in Fig. 9 has been built in lab. In the prototype, the control board is based on the 32-bit floating-point DSP Texas Instruments TMS320F28335. IGBT-Module FF200R12KT4 (Infineon) is used to construct the main circuit of the converter. The motor1 is the induction motor driven by the inverter. And the motor2 is a PMSM used as the load. The parameters corresponding to the experimental system are listed in Table III. In addition, the DC-link voltage is set to 300 V. The large current of the converter will lead to rapid deviation of the capacitor voltage. Considering the safety of the converter, the maximum torque is set to 3 N. m. The flux reference of the induction machine is 0.8 Wb, and the sample rate is 20 kHz. In the following experiments, the open-switch fault of IGBT is realized by turning off the IGBT deliberately.

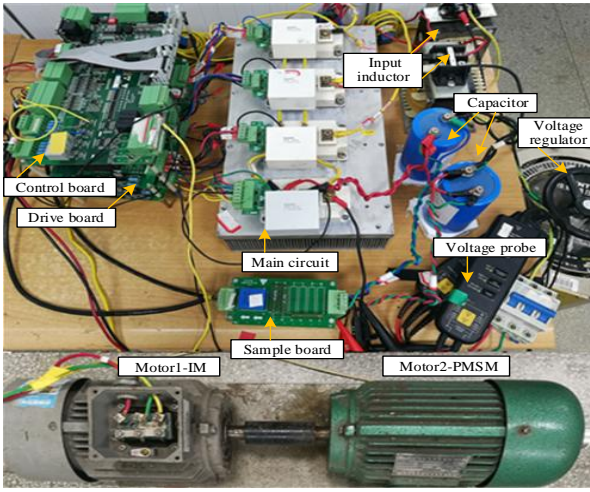


Fig. 9. Photograph of experimental prototype.

TABLE III
PARAMETERS USED IN THE EXPERIMENTS

Parameters	Description	Value
L	Input inductance	4.5mH
u_s	Input voltage	90 V
C_1, C_2	DC-link capacitance	600 μ F
L_m	Mutual inductance	0.335H
R_s	Stator resistance	6.4 Ω
R_r	Rotor resistance	4.8 Ω
L_s	Stator self-inductance	0.365H
L_r	Rotor self-inductance	0.365H
J	Moment of inertia	0.02kg.m ²
n_p	Number of pole pairs	2

A. Experimental Results of Rectifier

1) Results under Normal Condition

A good fault diagnosis method should have a low rate of false alarm and missed detection simultaneously. To test the false alarm rate under normal conditions, a loading procedure for the induction motor is constructed. Before $t=0.1$ s, the induction motor works under no load; At $t=0.1$ s, a load is added suddenly. The related experimental waveforms of the rectifier are shown in Fig. 10 (a). The waveforms from top to bottom are input current, residual and flag of fault, respectively. As seen, a small

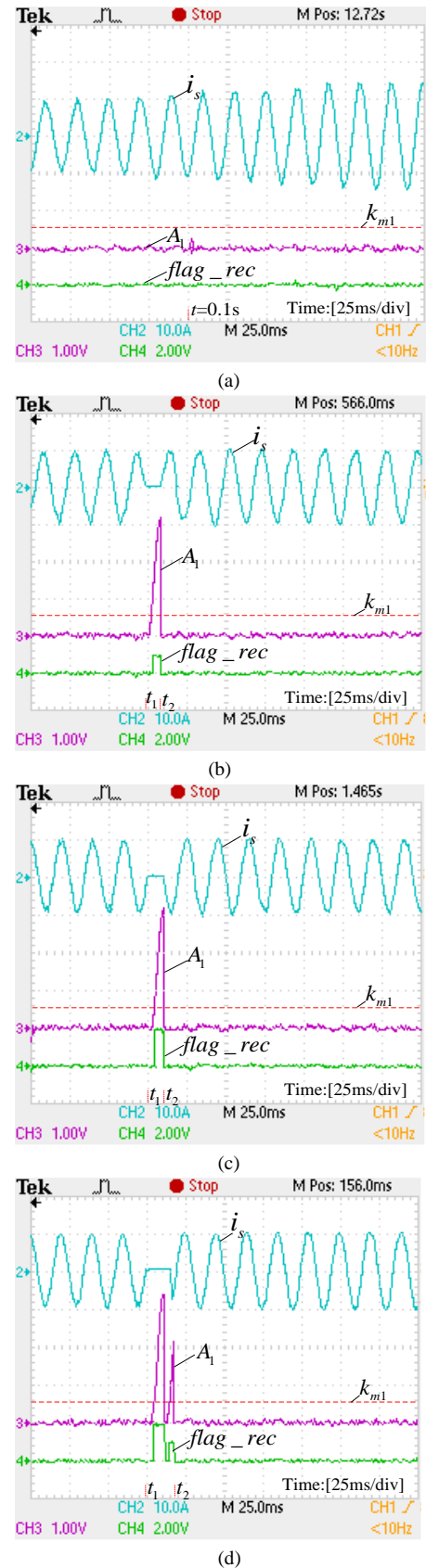


Fig. 10. Experimental waveforms: (a) normal condition; (b) T_7 is broken; (c) T_8 is broken; (d) T_7 and T_8 are broken.

increase in A_1 follows the loading event, but it is far less than the threshold and does not trigger the false alarm. Moreover,

both the steady residuals A_1 before and after $t=0.1s$ are small and almost equal to zero. Meanwhile, the measured flag of fault indicates that the drive system is in normal condition. Note that the encoding of the flag of the faults of rectifier and inverter is listed in Table IV. Where $flag_rec$ denotes the flag of fault in rectifier, $flag_inv$ denotes the flag of fault in inverter. This experiment indicates the proposed method is robust to the transients under normal conditions.

TABLE IV
FLAG OF FAULTS IN EXPERIMENTS

$flag_rec$ (V)	Fault switch	$flag_inv$ (V)	Fault switch
0	—	0	—
1	T_7	1	T_1
2	T_8	2	T_2
		3	T_3
		4	T_4
		5	T_5
		6	T_6

2) Results with Single Open-circuit Fault on Rectifier

In this experiment, the single open-switch fault of rectifier will be tested. Fig. 10(b) shows the measured waveforms when an open-switch fault happens on T_7 at $t= t_1$. As seen, a large residual (A_1) follows the fault and the input current is clamped to zero for half of the fundamental grid voltage period. According to the value of the flag of fault, the broken T_7 is detected precisely. Fig. 10(c) shows the measured waveforms when an open circuit fault happens at T_8 . Similarly, a large residual is found after the fault. Different from Fig. 10(b), the input current during the fault is less than zero. According to the flag of fault and Table IV, the fault switch T_8 is detected successfully.

3) Results with Double Open-circuit Faults on Rectifier

In this section, the cases with double open-switch fault will be tested. The fault starts at t_1 and ends at t_2 . Fig. 10(d) shows the experimental waveforms when the open-switch fault occurs simultaneously on the IGBT T_7 and T_8 . As seen, the input current is clamped to zero from the first zero crossing point of current after the fault to t_2 . When the residual exceeds the threshold, the open-switch fault on T_8 is firstly detected and isolated. After a while, the residual exceeds the threshold again, the fault on T_7 is also detected.

B. Experimental Results of Inverter

1) Results under Normal Condition

In this experiment, the effect of the proposed fault diagnosis for the inverter under normal condition will be evaluated. Fig. 11 shows the experimental results. The induction motor experiences three different states: start-up, no-load and loading processes. Fig. 11(a), (b) and (c) show the corresponding stator currents, speed and torque, residual and flag of fault. As shown in Fig. 11 (c), though a little fluctuation could be found during the start-up, the residuals under different stages are far less than threshold and do not trigger the false alarm. That is to say that

the proposed method is robust in different working conditions.

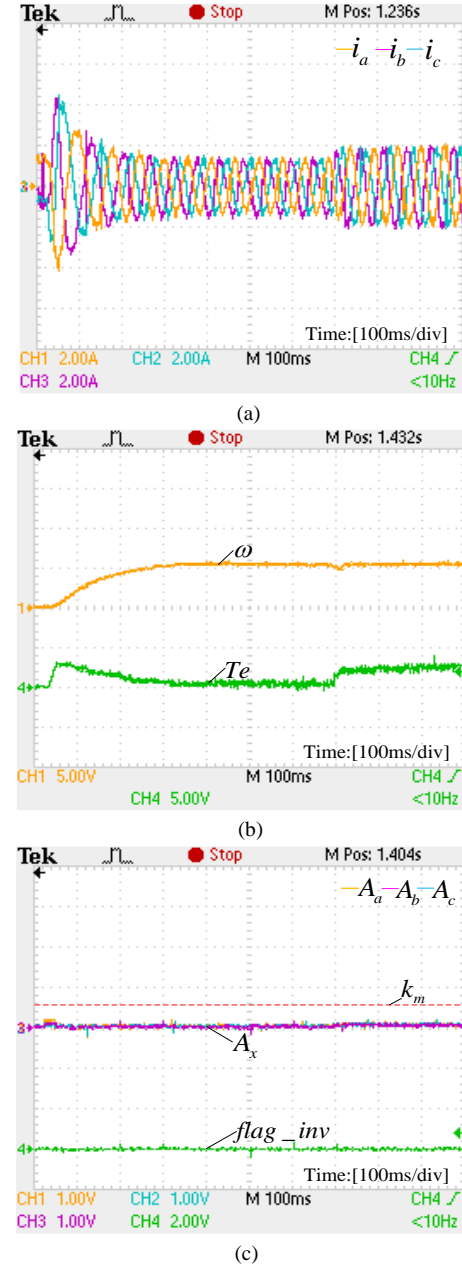


Fig.11. Experimental waveforms: (a) stator currents; (b) speed and torque of induction motor; (c) residual and flag of fault.

2) Results with Single Open-circuit Fault on Inverter

In this section, the cases under single open-switch fault will be tested. Fig. 12 shows the measured waveforms under the single open-switch fault which starts at t_1 and disappears at t_2 . Fig. 12(a) shows the stator current waveforms with $T_1=F$. Fig. 12(b) shows the resulted residuals (A_a , A_b and A_c) and the flag of faults. As seen, A-phase current is clamped to zero for a half of period. A_a is greater than A_b and A_c . According to the value of the flag, it can be deduced that T_1 is broken, which is in good agreement with Table II. Fig. 12(c) shows the stator currents with $T_2=F$. Fig. 12 (d) shows the residuals, where A_a is greater than A_b and A_c . Thus, it can be inferred that the fault happens on A-phase. As seen from Fig. 12(c), A-phase current is also

clamped to zero for a half of period, but it is different from that in Fig. 12(a). Combining with the information of residual ε_a , it can be inferred that T_2 is broken. Fig. 12(e) shows the stator currents with $T_3=F$. Fig. 12(f) shows the resulted residuals (A_a ,

A_b and A_c) and the flag of faults. As seen, B-phase current is clamped to zero for a half of period. A_b is greater than A_a and A_c . According to the information of the ε_b , it can be deduced that T_3 is broken, which is in good agreement with Table II.

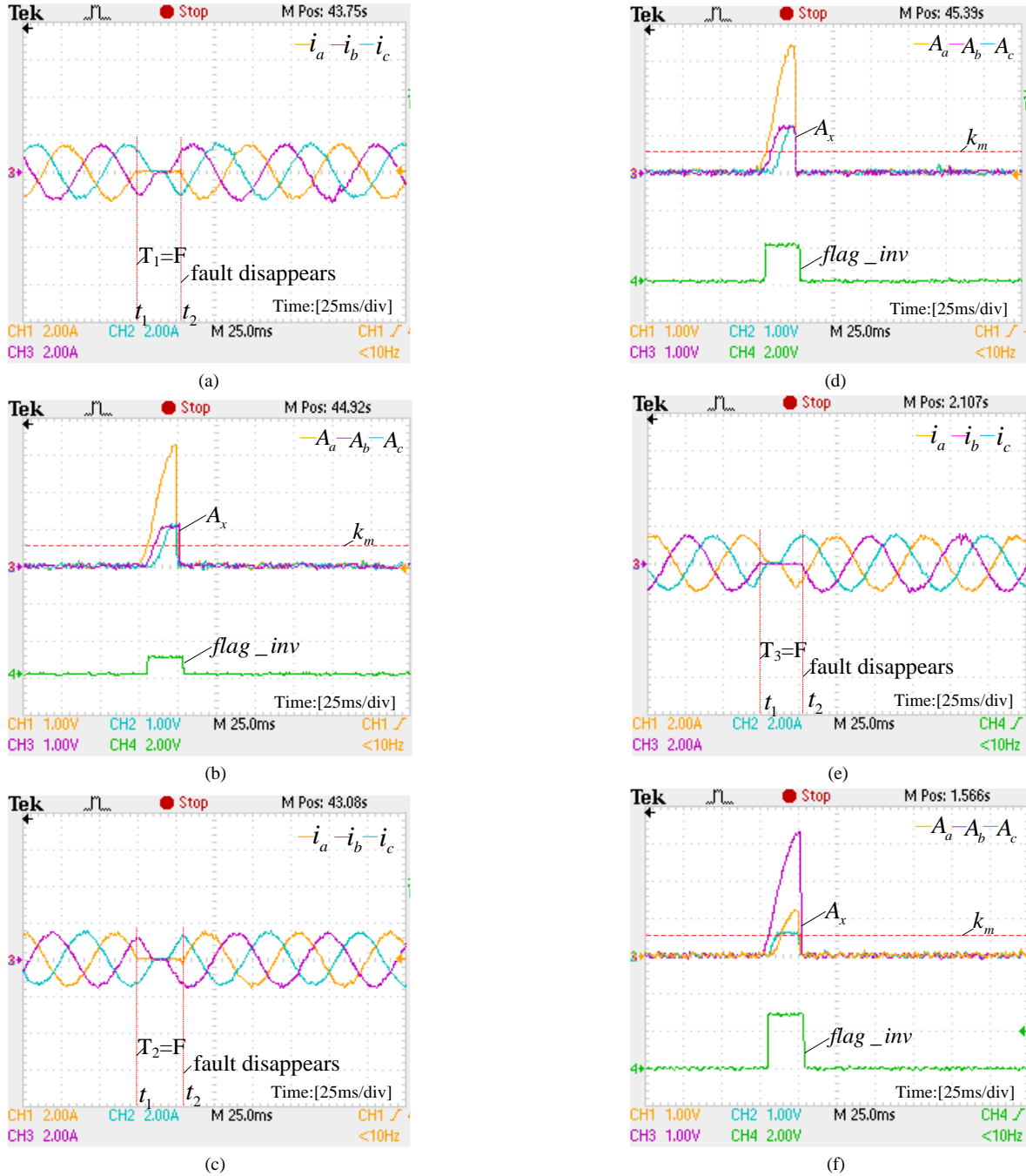


Fig. 12. Experimental waveforms: (a) stator currents with $T_1=F$; (b) residual and flag of fault with $T_1=F$; (c) stator currents with $T_2=F$; (d) residual and flag of fault with $T_2=F$; (e) stator currents with $T_3=F$; (f) residual and flag of fault with $T_3=F$.

3) Results under Double Faults on the Same Bridge Arm

In this experiment, the cases under double open-switch faults on the same bridge arm will be tested. Take the simultaneous fault of T_1 and T_2 as an example. Fig. 13(a) shows the stator currents with $T_1=T_2=F$. Fig. 13(b) shows the resulted residuals (A_a , A_b and A_c) and the flag of faults. As seen, the residuals exceed the threshold twice and the fault alarm is triggered twice

too. In the two fault alarms, A_a is greater than A_b and A_c , thus the fault happens on A-phase. Since ε_a is less than zero at $t=t_3$, it can be inferred that T_2 is broken. As ε_a is great than zero at $t=t_4$, it can be inferred that T_1 is broken. According to the measured flag of fault and Table IV, it is clear that the proposed method is effective to the double faults on the same bridge arm.

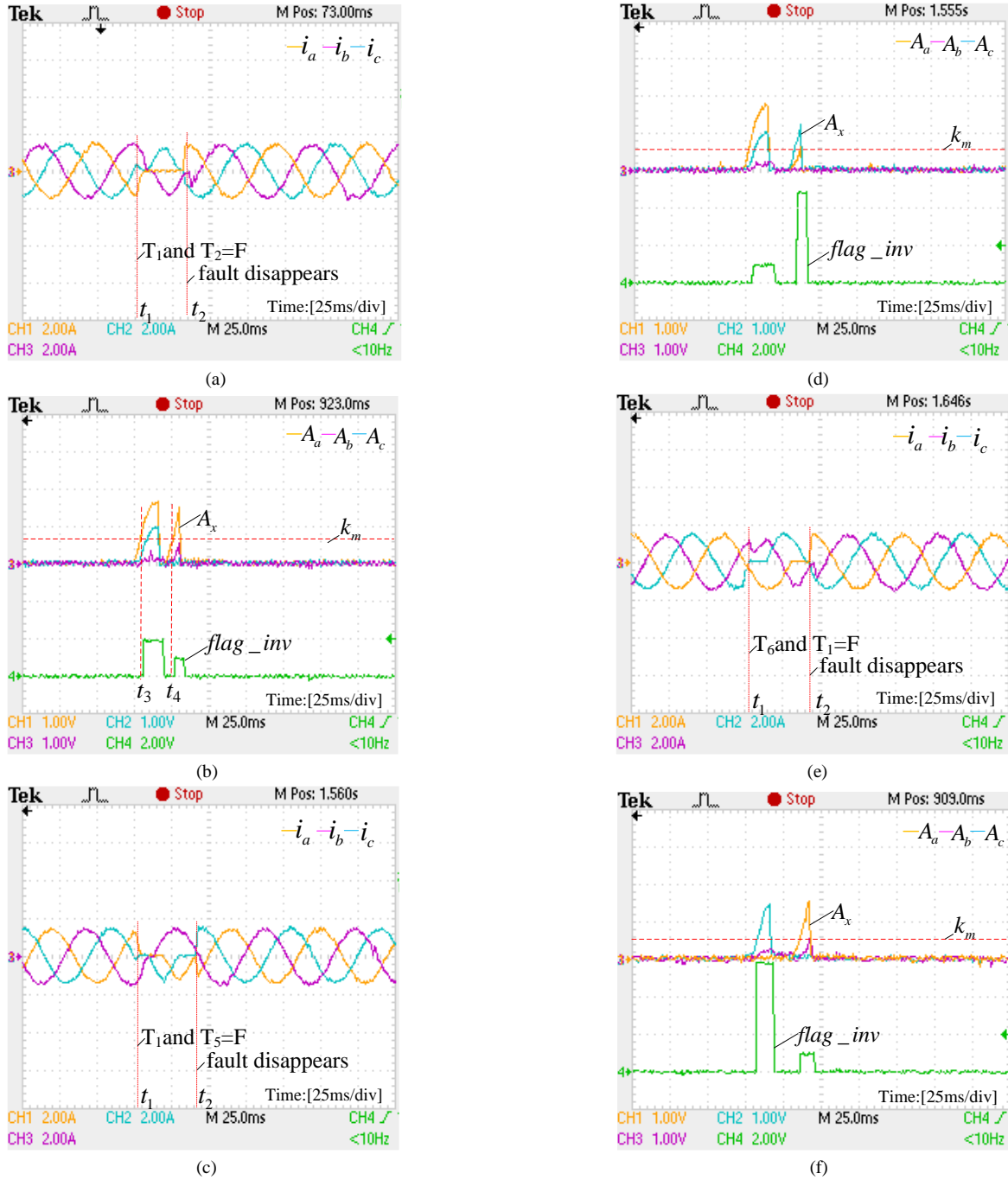


Fig. 13. Experimental waveforms: (a) stator currents with $T_1=F$ and $T_2=F$; (b) residual and flag of fault with $T_1=F$ and $T_2=F$; (c) stator currents with $T_1=F$ and $T_5=F$; (d) residual and flag of fault with $T_1=F$ and $T_5=F$; (e) stator currents with $T_6=F$ and $T_1=F$; (f) residual and flag of fault with $T_6=F$ and $T_1=F$.

4) Results under Double Faults on the Different Bridge Arms

In this experiment, the cases under double open-switch fault on the different bridge arm will be tested. Faults on different bridge arms can be divided into two cases: the double fault on the same side of different bridge arms (e.g. $T_1=T_5=F$) and the double fault on different sides of different bridge arms (e.g. $T_1=T_6=F$). Fig. 13(c) shows the stator currents in the case of $T_1=T_5=F$. Fig. 13(d) shows the resulted residuals (A_a , A_b and A_c) and the flag of faults. As seen, the residuals conditions correspond to the states ① and ③ in the Table II. Thus, it can be deduced that the fault happens on T_1 and T_5 . Fig. 13(e) and (f)

show the stator currents and related residuals with $T_1=T_6=F$. As seen, the residuals conditions correspond to the states ① and ⑥ in the Table II, which indicates that the proposed fault diagnosis is valid in this case.

VI. CONCLUSION

This paper presents a simple and reliable fault diagnosis method based on moving integration filter for three-phase induction motor drive systems. The experimental results show that this method could realize fault detection and fault isolation for the induction motor drive system accurately in the case of

single or double open-switch faults. And the main advantages of the proposed method are summarized as follow:

1) No extra sensors are required. Thus, it is a cost-effective approach;

2) The computation burden of this diagnosis method is small. Since the fault diagnosis method is based on the framework of model predictive control, many shared data could be fully utilized, much computation time can be saved.

3) This method is robust and reliable. As the moving integration filter-based residuals are used, it is easy to determine a proper threshold to guarantee a low rate of false alarm and missed detection.

Based on the above merits, it is clear that this method is suitable for the applications such as electric vehicle, electric locomotive, where high reliability is requested.

REFERENCES

- [1] W. Wang, X. B. Chen, and J. M. Wang, "Motor/Generator Applications in Electrified Vehicle Chassis-A Survey," *IEEE Trans. Transportation Electrification*, vol. 5, no. 3, pp. 584–601, Sep. 2019.
- [2] A. C. Noroés Maia, and C. B. Jacobina, "Single-phase ac-dc-ac topology for grid overvoltage and voltage harmonic mitigation," *IET Power Electron.*, vol. 10, no. 12, pp. 1626–1637, Oct. 2017.
- [3] B. Tabbache, M. Benbouzid, A. Kheloui, J. M. Bourgeot, and A. Mamoune, "An improved fault-tolerant control scheme for PWM inverter-fed induction motor-based EVs," *ISA Trans.*, vol. 52, no. 6, pp. 862–869, 2013.
- [4] Y. Song, and B. Wang, "Survey on Reliability of Power Electronic Systems," *IEEE Trans. Power Electron.*, vol. 28, no. 1, pp. 591–604, Jan. 2013.
- [5] B. Lu and S. K. Sharma, "A Literature Review of IGBT Fault Diagnostic and Protection Methods for Power Inverters," *IEEE Trans. Ind. Appl.*, vol. 45, no. 5, pp. 1770–1777, Sep.-oct. 2009.
- [6] D. U. Campos-Delgado, D. R. Espinoza-Trejo, and E. Palacios, "Fault-tolerant control in variable speed drives: a survey," *IET Electr. Power Appl.*, vol. 2, no. 2, pp. 121–134, Mar. 2008.
- [7] S. Q. Shi, Y. Sun, M. Su, and R. Y. Che, "Hybrid predictive control strategy for a low-cost converter-fed IM drive," *IET Electr. Power Appl.*, vol. 12, no. 4, pp. 581–587, Apr. 2018.
- [8] B. A. Welchko, T. A. Lipo, T.M. Jahns, et al., "Fault tolerant three-phase AC motor drive topologies: a comparison of features, cost, and limitation," *IEEE Trans. Power Electron.*, vol. 19, no. 4, pp. 1108–1116, Jul. 2004.
- [9] A. M. S. Mendes, A. J. M. Cardoso and E. S. Saraiva, "Voltage source inverter fault diagnosis in variable speed AC drives, by Park's vector approach," *1998 Seventh International Conference on Power Electronics and Variable Speed Drives*, London, UK, 1998, pp. 538–543.
- [10] D. Diallo, M. E. H. Benbouzid, D. Hamad and X. Pierre, "Fault detection and diagnosis in an induction Machine drive: a pattern recognition approach based on concordia stator mean current vector," in *IEEE Transactions on Energy Conversion*, vol. 20, no. 3, pp. 512–519, Sep. 2005.
- [11] W. Sleszynski, J. Nieznanski, and A. Cichowski, "Open-transistor fault diagnostics in voltage-source inverters by analyzing the load currents," *IEEE Trans. Ind. Electron.*, vol. 56, no. 11, pp. 4681–4688, Nov. 2009.
- [12] J. O. Estima and A. J. M. Cardoso, "A new algorithm for real-time multiple open-circuit fault diagnosis in voltage-fed PWM motor drives by the reference current errors," *IEEE Trans. Ind. Electron.*, vol. 60, no. 8, pp. 3496–3505, Aug. 2013.
- [13] N. M. A. Freire, J. O. Estima, and A. J. M. Cardoso, "Open-circuit fault diagnosis in PMSG drives for wind turbine applications," *IEEE Trans. Ind. Electron.*, vol. 60, no. 9, pp. 3957–3967, Sep. 2013.
- [14] J. O. Estima and A. J. Marques Cardoso, "A New Approach for Real-Time Multiple Open-Circuit Fault Diagnosis in Voltage-Source Inverters," in *IEEE Transactions on Industry Applications*, vol. 47, no. 6, pp. 2487–2494, Nov.-Dec. 2011.
- [15] Q. An, L. Sun and L. Sun, "Current Residual Vector-Based Open-Switch Fault Diagnosis of Inverters in PMSM Drive Systems," in *IEEE Transactions on Power Electronics*, vol. 30, no. 5, pp. 2814–2827, May 2015.
- [16] H. T. Eickhoff, R. Seebacher, A. Muetze and E. G. Strangas, "Enhanced and Fast Detection of Open-Switch Faults in Inverters for Electric Drives," in *IEEE Transactions on Industry Applications*, vol. 53, no. 6, pp. 5415–5425, Nov.-Dec. 2017.
- [17] I. Jlassi, J. O. Estima, S. K. El Khil, N. M. Bellaaj and A. J. M. Cardoso, "A Robust Observer-Based Method for IGBTs and Current Sensors Fault Diagnosis in Voltage-Source Inverters of PMSM Drives," in *IEEE Transactions on Industry Applications*, vol. 53, no. 3, pp. 2894–2905, May-June 2017.
- [18] R. L. de Araujo Ribeiro, C. B. Jacobina, E. R. C. da Silva and A. M. N. Lima, "Fault detection of open-switch damage in voltage-fed PWM motor drive systems," in *IEEE Transactions on Power Electronics*, vol. 18, no. 2, pp. 587–593, Mar. 2003.
- [19] M. Trabelsi, M. Boussak, and M. Gossa, "PWM-Switching pattern-based diagnosis scheme for single and multiple open-switch damages in VSI-fed induction motor drives," *ISA Trans.*, vol. 51, no. 2, pp. 333–344, 2012.
- [20] Z. Huang, Z. Wang and H. Zhang, "A Diagnosis Algorithm for Multiple Open-Circuited Faults of Microgrid Inverters Based on Main Fault Component Analysis," in *IEEE Transactions on Energy Conversion*, vol. 33, no. 3, pp. 925–937, Sep. 2018.
- [21] H. Dan *et al.*, "Error-Voltage-Based Open-Switch Fault Diagnosis Strategy for Matrix Converters with Model Predictive Control Method," in *IEEE Transactions on Industry Applications*, vol. 53, no. 5, pp. 4603–4612, Sep.-Oct. 2017.
- [22] D. Zhou, S. Yang and Y. Tang, "A Voltage-Based Open-Circuit Fault Detection and Isolation Approach for Modular Multilevel Converters With Model-Predictive Control," in *IEEE Transactions on Power Electronics*, vol. 33, no. 11, pp. 9866–9874, Nov. 2018.
- [23] I. González-Prieto, M. J. Duran, N. Rios-Garcia, F. Barrero and C. Martín, "Open-Switch Fault Detection in Five-Phase Induction Motor Drives Using Model Predictive Control," in *IEEE Transactions on Industrial Electronics*, vol. 65, no. 4, pp. 3045–3055, April 2018.
- [24] S. Khomfoi and L. M. Tolbert, "Fault Diagnosis and Reconfiguration for Multilevel Inverter Drive Using AI-Based Techniques," in *IEEE Transactions on Industrial Electronics*, vol. 54, no. 6, pp. 2954–2968, Dec. 2007.
- [25] P. Cortes, M. P. Kazmierkowski, R. M. Kennel, D. E. Quevedo, and J. Rodriguez, "Predictive control in power electronics and drives," *IEEE Trans. Ind. Electron.*, vol. 55, no. 12, pp. 4312–4324, Dec. 2008.
- [26] S. Vazquez, J. Rodriguez, M. Rivera, et al., "Model predictive control for power converters and drives: advances and trends," *IEEE Trans. Ind. Electron.*, vol. 64, no. 2, pp. 935–947, Feb. 2017.
- [27] S. Shao, A. Ehsan, B. Farhad, and M. Richard, "Stator-flux-oriented vector control for brushless doubly fed induction generator," *IEEE Trans. Ind. Electron.*, vol. 56, no. 10, pp. 4220–4228, Oct. 2009.
- [28] Y. X. Su, C. H. Zheng, P. C. Mueller, and B. Y. Duan, "A simple improved velocity estimation for low-speed regions based on position measurements only," *IEEE Trans. Control Systems Technology*, vol. 14, no. 5, pp. 937–942, Sep. 2006.
- [29] L. Harnefors, and H. P. Nee, "A General Algorithm for Speed and Position Estimation of AC Motors," *IEEE Trans. Ind. Electron.*, vol. 47, no. 1, pp. 77–83, Feb. 2000.



Shuqi Shi was born in Hunan, China, in 1986. He received the B.S. degree in electrical engineering from Hunan Institute of Engineering, Xiangtan, China, in 2009, and the M.S. degree in electrical engineering from Hunan University, Changsha, China, in 2012. He is currently working toward the Ph.D. degree in control science and engineering at Central South University, Changsha, China.

His current research interests include motor control, model predictive control, fault diagnosis.



Yao Sun (M'13) was born in Hunan, China, in 1981. He received the B.S., M.S. and Ph.D. degrees from Central South University, Changsha, China, in 2004, 2007 and 2010, respectively. He has been a Professor with the School of Automation, Central South University, China.

His research interests include matrix converter, micro-grid and wind energy conversion system.



Xing Li was born in Hunan, China, in 1988. She received the B.S. and Ph.D. degrees from Central South University, Changsha, China, in 2009 and 2014, respectively. She is currently an Associate Professor with the College of Electrical and Information Engineering, Hunan University, Changsha, China.

Her research interests include power electronic converter and wind energy conversion system.



Hanbing Dan was born in Hubei, China, in 1991. He received the B.S. degree in Automation, and Ph.D. degree in Control Science and Engineering from Central South University, Changsha, China, in 2012, and 2017, respectively. He was a visiting researcher in Faculty of Engineering at the University of Nottingham, United Kingdom during 2017. He is currently an associate professor with the School of Automation, Central South University, China.

His research interests include power converter, motor control, model predictive control, fault diagnosis.



Mei Su was born in Hunan, China, in 1967. She received the B.S., M.S. and Ph.D. degrees from the School of Information Science and Engineering, Central South University, Changsha, China, in 1989, 1992 and 2005, respectively. She has been a Full Professor with the School of Automation, Central South University, China. She is currently an Associate Editor of the IEEE Transactions on Power Electronics.

Her research interests include matrix converter, adjustable speed drives, and wind energy conversion system.